HiSST: 2nd International Conference on
High-Speed Vehicle Science & Technology
11–15 September 2022, Bruges, Belgium

Preliminary analysis of multi-dimensional material response of DragonFly heat shield

Bibin Joseph[1], Raghava S.C. Davuluri [2], Aleksander L. Zibitsker[3], Alexandre Martin[4]

Abstract

A multi-dimensional material response simulation of the heat shield of the DragonFly capsule is performed. The material response includes mass, momentum, and energy equations. The heat flux and pressure profiles extracted from flow field simulations along the trajectory are used as boundary conditions for simulation. The results from the simulation are presented and are thoroughly studied to evaluate the complete behavior of the heat shield during the entry.

Keywords: *heat shield, ablation, DragonFly, Titan, material response, hypersonics*

1. Introduction

DragonFly is a relocatable lander mission to Titan, Saturn's moon, which aims to study its organic-rich ocean world. Titan has an earth-like atmosphere with colder temperature of -179°C, and atmospheric composition of roughly 95% nitrogen and 5% methane. Titan has a combination of low gravity and high density atmosphere, when compared to earth. This results in a long reentry phase with equal contributions of convective and radiative heat fluxes at the peak, on the forebody. Therefore, the thermal response of the forebody is required for accurate Thermal Protection System (TPS) sizing, and is achieved through both numerical and experimental analysis.

An charring ablative TPS material is used as the forebody heat shield. Charring ablators are porous fibrous materials infused with organic resin [1]. Under severe aerodynamic heating conditions, the resin undergoes thermal decomposition, which results in pyrolysis gas flow through the material and subsequent injection into the boundary layer. This convoluted process prevents some of the energy to reach the surface, and, through mass removal, prevents the remaining energy to become thermal energy [2].

In the past, Brandis et al. [3] performed aerothermodynamic analysis for flow over DragonFly at different trajectory points to evaluate the heat flux (both convective and radiative) acting on the forebody. The heat flux profiles were used by Banerjee et al. [4] to study the material response along the stagnation point. Similar study was also conducted by Sirmalla et al. [5]. However, these studies were conducted in 1D.

In this study, we performed a preliminary analysis of multi-dimensional material response of DragonFly on Titan's atmosphere. We consider the composition of the atmosphere to nominally be 98.2 N_2 : 1.6 CH_4 : 0.1 H_2: 0.1 Ar. A chemical equilibrium model accounting for interactions between carbon-based ablative material (TACOT) and Titan's atmospheric species is considered to predict the surface behavior of the material under entry heating.

[1]*Mechanical and Aerospace Eng., University of Kentucky, Lexington, KY, josephbibin@uky.edu*
[2]*Mechanical and Aerospace Eng., University of Kentucky, Lexington, KY, raghava.davuluri@uky.edu*
[3]*Mechanical and Aerospace Eng., University of Kentucky, Lexington, KY, alex.zibitsker@uky.edu*
[4]*Mechanical and Aerospace Eng., University of Kentucky, Lexington, KY, alexandre.martin@uky.edu*

2. Methodology

2.1. KATS – MR

The material response for this study is performed using Kentucky Aerothermodynamics and Thermal-response System (KATS) [6, 7] that uses a finite volume approach to solve the governing equations. These are discretized first order in time and second-order in space, and take the form of:

$$\frac{\partial \mathbf{Q}}{\partial t} + \nabla \cdot (\boldsymbol{\mathcal{F}} - \boldsymbol{\mathcal{F}_d} - \boldsymbol{\mathcal{F}_g}) = \mathbf{S}, \tag{1}$$

where, **Q** is conservative variable vector, $\boldsymbol{\mathcal{F}}$ is advective flux matrix, $\boldsymbol{\mathcal{F}_d}$ is diffusive flux matrix, and $\boldsymbol{\mathcal{F}_d}$ is the grid motion flux matrix. **S** is the source term [8, 9]. The conservative variables and the source term vectors are of the form:

$$\mathbf{Q} = \begin{pmatrix} \phi\rho_{g_1} \\ \vdots \\ \phi\rho_{g_{ngs}} \\ \rho_s \\ \vdots \\ \rho_{s_{nss}} \\ \phi\rho_g \mathbf{v}^T \\ \phi\rho E_g + E_s \end{pmatrix}, \qquad \mathbf{S} = \begin{pmatrix} \dot{\omega}_{g_1} \\ \vdots \\ \dot{\omega}_{g_{ngs}} \\ \dot{\omega_s} \\ \vdots \\ \dot{\omega_{s_{nss}}} \\ \mathbf{D}^T \\ S_D \end{pmatrix} \tag{2}$$

where $\dot{\omega}_g$ is the mass production rate of species g, ϕ is the porosity of the material, ρ is the density of material, **v** is the gas velocity vector, E is energy per unit volume. The diffusive effects (Darcy effects) on the momentum equation by the porous structure are accounted through the vector **D**, and S_D is the diffusive source term in the energy equationThe subscript ngs is for the number of gas species, and nss is for the number of solid species. The subscripts g and s represent the gas and solid states. Similarly, the convective and diffusive flux matrices in equation one are as follows,

$$\boldsymbol{\mathcal{F}} = \begin{pmatrix} \phi\rho_{g_1}\mathbf{v} \\ \vdots \\ \phi\rho_{g_{ngs}}\mathbf{v} \\ 0 \\ \vdots \\ 0 \\ \phi\rho_g \mathbf{v}\mathbf{v}^T + \boldsymbol{\mathcal{I}}p \\ \phi\rho_g H \end{pmatrix} \qquad \boldsymbol{\mathcal{F}_d} = \begin{pmatrix} \\ \\ \mathbf{0} \\ \\ \\ \mathbf{F}_{cond} \end{pmatrix} \tag{3}$$

where $\boldsymbol{\mathcal{I}}$ is the identity matrix, p is the static pressure, H is the gas enthalpy, and $\mathbf{F}_{cond}$ is the conductive heat flux vector. The solver uses PETSC, ParMETIS, and MPI to solve the linear system of equations, domain decomposition, and message passing, respectively.

2.2. Boundary conditions

The heat flux is applied using an aerothermodynamic boundary condition according:

$$q_{\text{aero}} = \rho_e u_e C_{h0} \Omega_{blw} (h_r - h_w) \tag{4}$$

where q_{aero} is the aerodynamic heat flux, ρ_e and u_e are the boundary layer edge density and velocity, C_{h0} is the convective heat transfer coefficient, Ω_{blw} is the blowing correction for the advective flux [6], h_r is recovery enthalpy, and h_w is the wall enthalpy.

The flow field simulation data does not provide the radiation heat flux and we simply add it to the total heat flux, and not account for potential volumetric heating[10, 11, 12]. The heat transfer coefficient is calculated at the beginning of the simulation using:

$$\rho_e u_e C_{h0} = q_{\text{CFD}}/(h_r - h_w) \tag{5}$$

where q_{CFD} is the cold wall heat flux provided from the flow field simulation. The wall enthalpy h_w is calculated using the temperature computed by the material response solver, and the recovery enthalpy h_r is approximated to the freestream enthalpy at the each trajectory points. It is to note that the use of the freestream kinetic energy for calculating the recovery enthalpy is not entirely accurate, especially in the early entry trajectory points where the low pressure break the continuum hypothesis. For the pyrolysis gas properties, a chemical equilibrium model is used. For the composition of the atmosphere, the data from the Cassini probe is considered [13]. The material properties of TACOT [14] are used for the simulation. A chemistry model – the so-called B' table – involving the gas-surface reactions between Titan's atmospheric species and TACOT [14] is used for the simulation.

3. Results and Discussion

The material response simulation is computed along the trajectory of the DragonFly. The trajectory points considered for the thermal response simulation are shown in Fig. 1. It should be noted that the trajectory point at 235.82 seconds corresponds to peak heating.

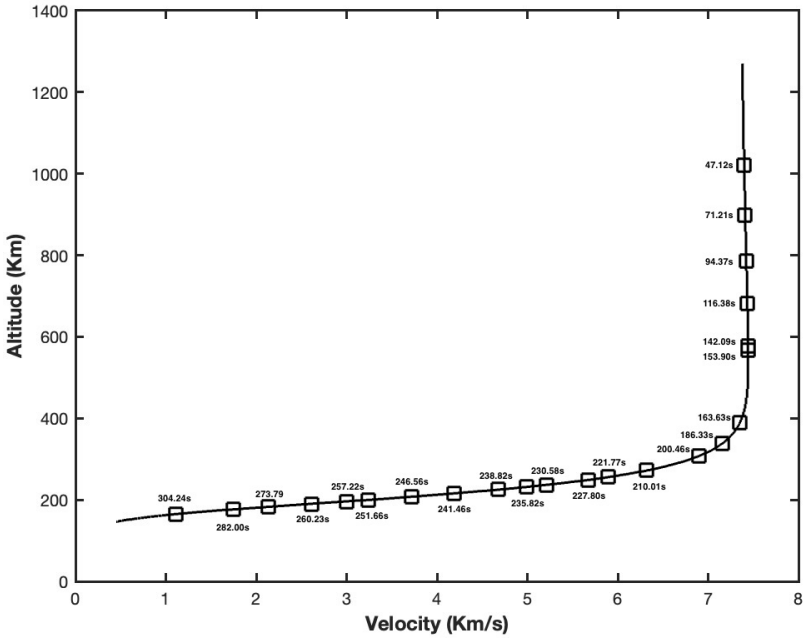

Fig 1. Trajectory of DragonFly's Titan entry

The heat flux and pressure at the stagnation point were extracted from the flow field simulation. The heat flux and pressure profiles at the stagnation point as a function of flight time are illustrated in Fig. 2. The heat flux at the stagnation point increases from zero to a maximum value of 187.9 W/cm^2 at 235.82 seconds, and then decreases to zero along the trajectory as seen in Fig. 2(a). On the contrary, the pressure at the stagnation point increases from zero and reaches the maximum value of 272 Pa at the end of the trajectory as shown in Fig. 2(b).

The material response is simulated for the complete trajectory. The heat flux and pressure profiles along the DragonFly's surface at different trajectory points are considered and the profiles obtained at a few

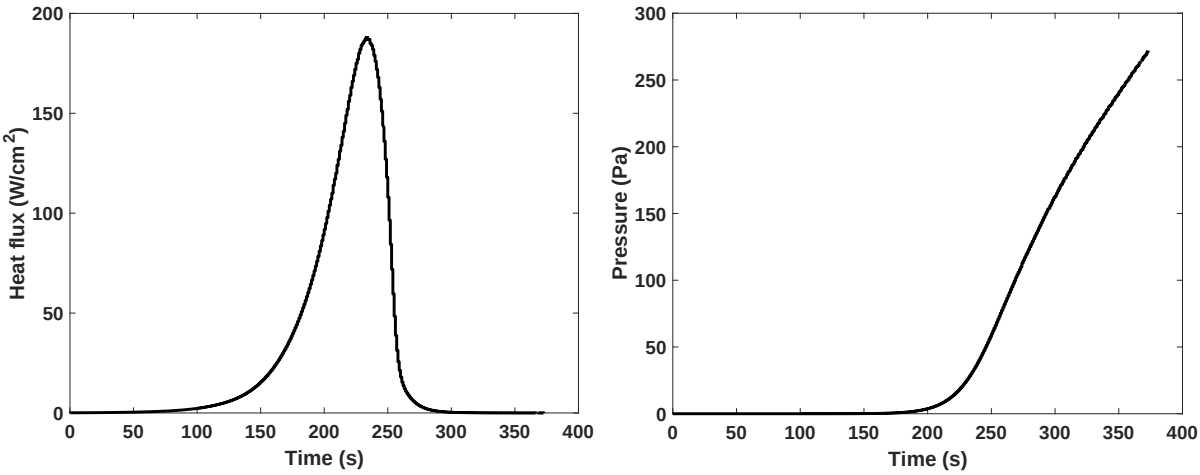

(a) Heat flux profile as a function of time of flight (b) Pressure profile as a function of time of flight

Fig 2. Heat flux and pressure profiles at the stagnation point along the DragonFly's trajectory

trajectory points are presented in Fig. 3. Due to low heat flux and pressure during the initial part of the entry, the simulation begins at 47.12 seconds, to avoid numerical issues. The simulation starts with the heat flux and pressure profile at 47.12 seconds as the boundary conditions at the heating surface. At each time step, interpolated values of heat flux and pressure profiles of successive trajectory points as a function of time are given as boundary conditions till the end of the trajectory.

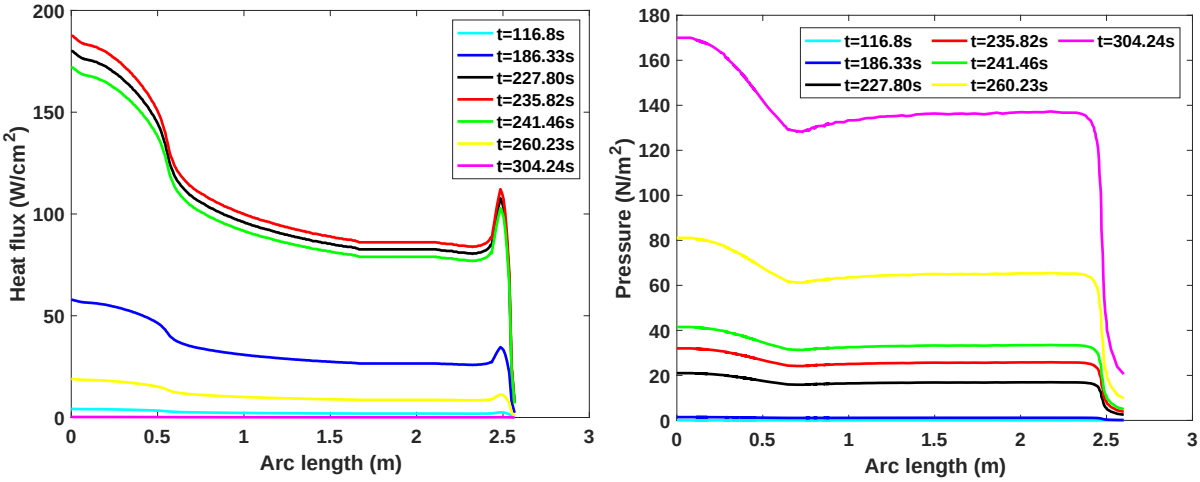

(a) Heat flux profiles along the surface at different time of flights (b) Pressure profiles along the surface at different time of flights

Fig 3. Heat flux and pressure profiles along the surface at different time of flights

Using the heat flux profile at the stagnation point as shown in Fig. 2(a), the heat transfer coefficient, as defined in Eq. 4, is calculated at each trajectory point and its profile is presented in Fig. 4. The calculated heat transfer coefficient is used to compute the aerothermodynamic heating flux at the heating surface.

The temperature histories at different Thermocouple (TC) locations are illustrated in Fig. 6. The TC

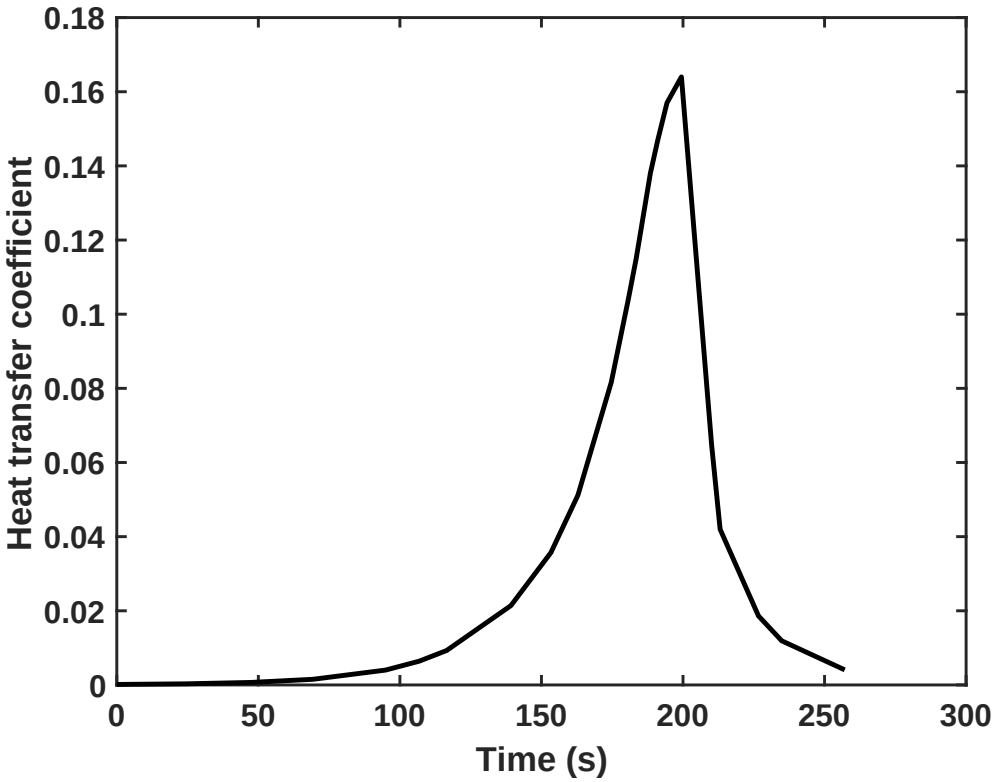

Fig 4. Heat transfer coefficient for the aeroheating boundary condition

Table 1. Virtual Thermocouple locations

TC#	Coordinates, m
1	$(0.00000, 0.00000, 0.0)$
2	$(0.00000, -0.00145, 0.0)$
3	$(0.00000, -0.00293, 0.0)$
4	$(0.00000, -0.00877, 0.0)$
5	$(0.00000, -0.01609, 0.0)$
6	$(0.00000, -0.03657, 0.0)$
7	$(0.35035, -0.04934, 0.0)$
8	$(0.71981, -0.21585, 0.0)$
9	$(1.39697, -0.61023, 0.0)$
10	$(1.43919, -0.63466, 0.0)$
11	$(2.13026, -1.03729, 0.0)$
12	$(2.16013, -1.05802, 0.0)$
13	$(2.20007, -1.10447, 0.0)$
14	$(2.22589, -1.16551, 0.0)$

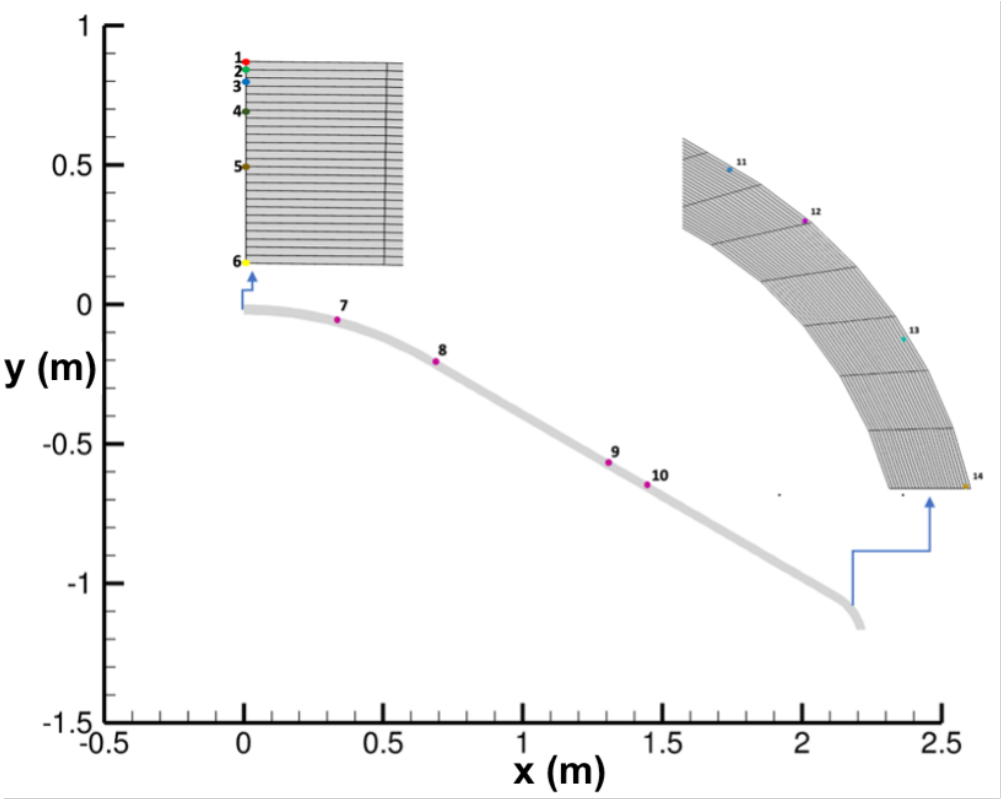

Fig 5. Thermocouple locations

locations are presented in Table 1 and the pictorial representation of their locations in the heat shield is shown in Fig. 5. In the Fig. 6(a), it can seen that the temperature increases for TC's along the stagnation line with TC 1 reaching a maximum of 2040 K. The maximum temperatures reached by other TC's along the stagnation line decreases with depth. It is interesting to note that TC 6, which is at the end of heat shield, reaches around 600 K by the end of simulation time. Similar behavior is observed for TC's along the shoulder with temperatures of each TC reaching around 600 K at the end of the simulation time. However, it is interesting to note that the temperature histories of TC's (9, 10, 14), and (11, 12, 13), respectively, are almost same as shown in Fig. 6.

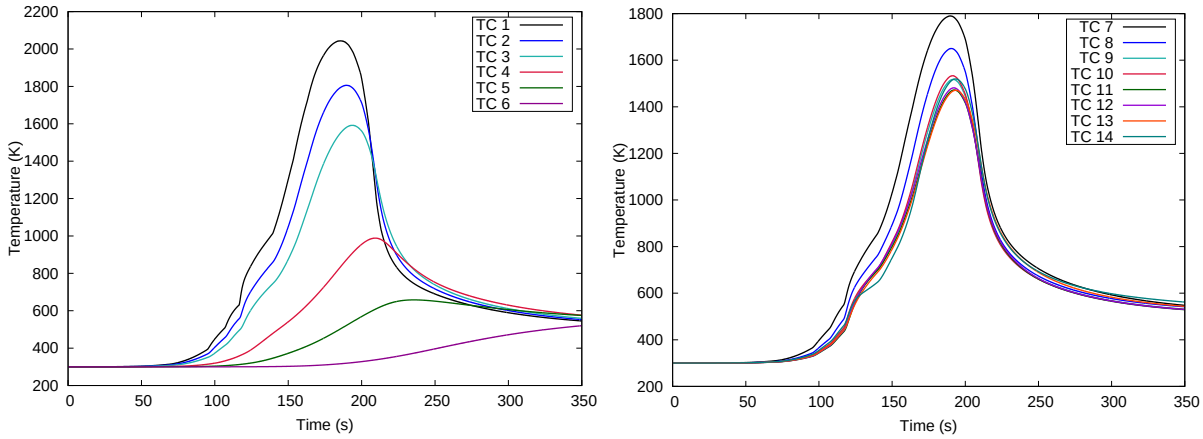

(a) Temperature histories along the stagnation line

(b) Temperature histories along the shoulder

Fig 6. Temperature histories at various thermocouple locations

The temperature profiles along the surface of DragonFly's heat shield at different trajectory points are presented in Fig. 7. It can seen that the temperature profile increases to a maximum value at peak heating trajectory point and decreases to around 600 K at the end of simulation time.

The different components of heat flux along the surface at different trajectory points is shown in Fig. 8. The heat flux components consist of aerothermodynamic heat flux (q_{aero}), re-radiative heat flux (q_{rerad}), pyrolysis gas heat flux (q_{pyro}), and conduction heat flux (q_{cond}). It can be observed from Fig. 8 that, as expected, the two prominent heat flux components are aerothermodynamic and re-radiative heat fluxes. It should be noted that the time points shown in Fig. 8 represent the simulation time points and not the trajectory points.

Figure 9 shows the pyrolysis gas heat and blowing fluxes along the surface at different trajectory time points. These fluxes are directly linked with the pressure field. The blowing correction obtained using the low pressure during the early entry introduced some disparity in the chemical equilibrium calculation. This discrepancy has resulted noise in the pyrolysis gas heat flux and mass flux, as observed in figure 9(a) and (b), respectively.

Finally, it is important to note that even though the code has the ability to model surface recession, none is observed. This result is certainly expected for such a relatively mild entry within a oxygen deprived atmosphere. The surface temperature, although high, is not enough to trigger sublimation. It is, however, possible that some of the oxygen present in the pyrolysis gas ablates the carbon fibers from within. The current modeling approach does not account for this phenomenon, but will be investigated in the near future.

4. Conclusion

A multi-dimensional material response simulation is performed on a DragonFly heat shield. The material response simulation included solution of mass, momentum, and energy equations. Heat flux and pres-

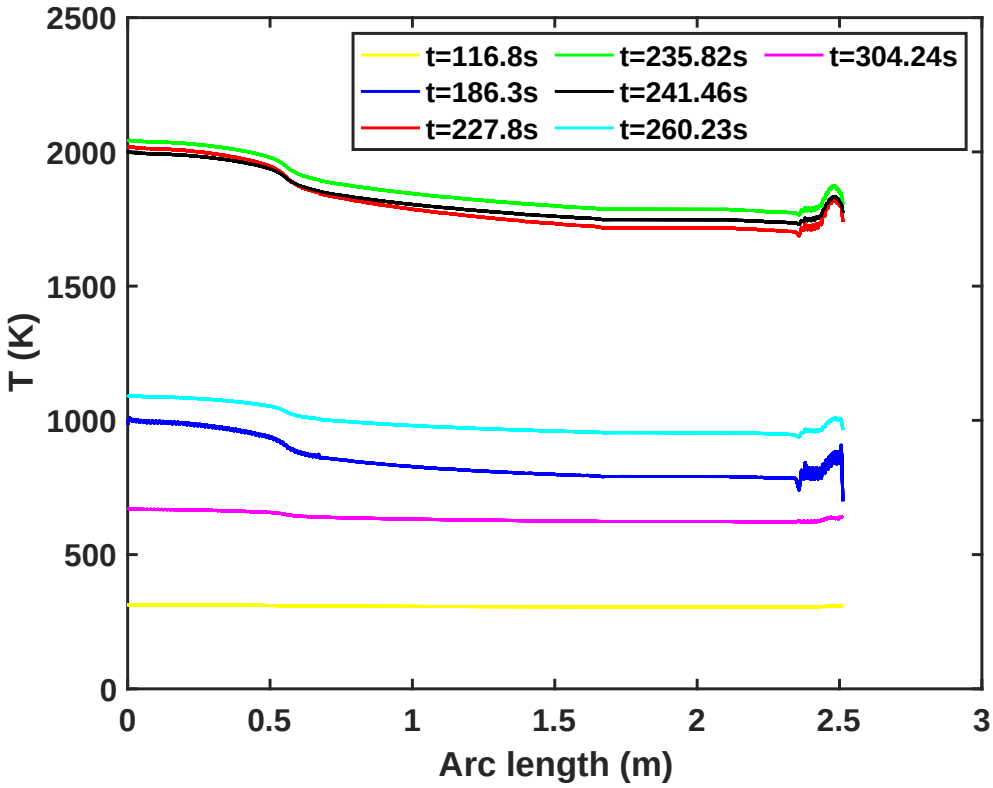

Fig 7. Temperature profiles along the surface at different trajectory points

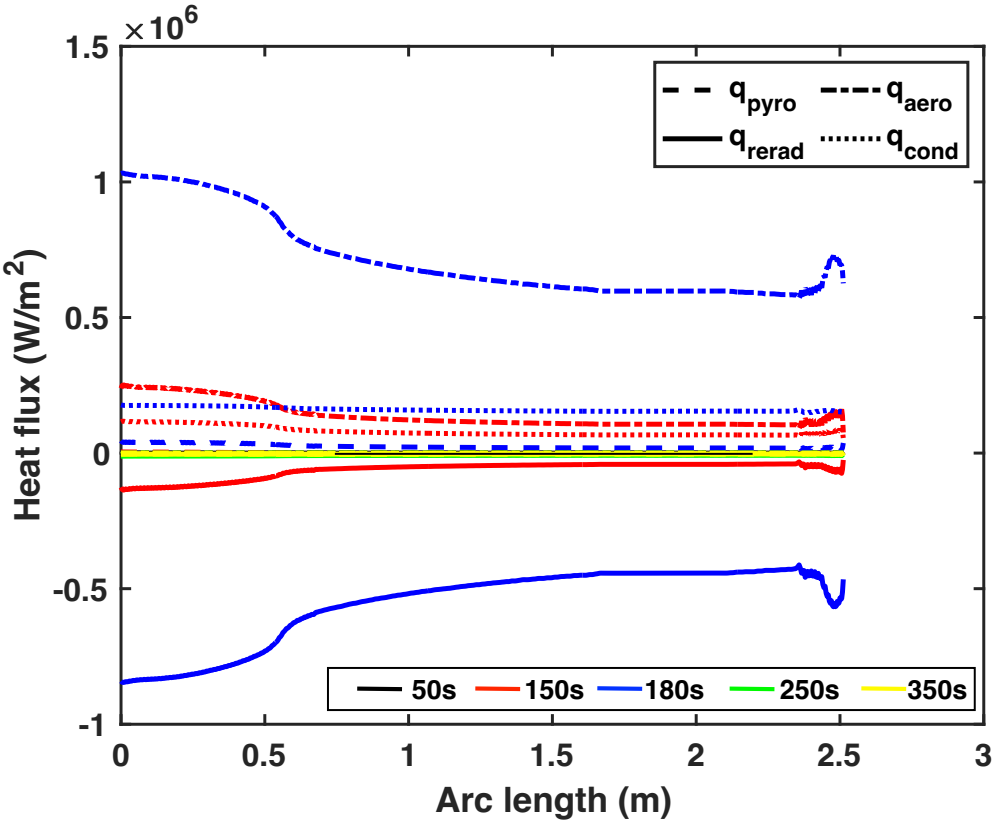

Fig 8. Heat flux components along the surface at different trajectory points

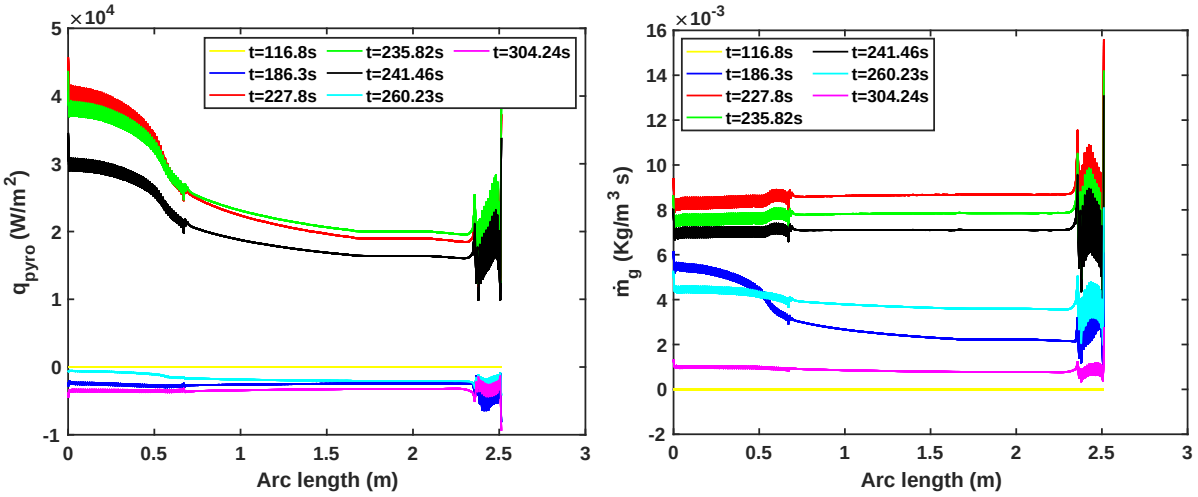

(a) Pyrolysis gas heat flux profiles along the surface at different trajectory points

(b) Pyrolysis gas blowing flux profiles along the surface at different trajectory points

Fig 9. Pyrolysis gas heat flux and blowing flux profiles along the surface at different trajectory points

sure profiles were used to distribute the stagnation point at different trajectory points over then entire surface. These profiles were given as boundary condition to the heating surface and the simulation was run for the total trajectory. The material properties of TACOT were used for the simulation.

The temperature histories at the thermocouple locations and temperature profiles along the heating surface at different trajectory points were presented. The thermal response of the heat shield showed expected behavior with the stagnation point reaching a maximum value of 2040 K and bondline temperature reaching around 600 K. It was observed that the aerothermodynamic and re-radiative heat fluxes are major contributors of heat flux during the simulation.

With the simulation performed, the material response of the DragonFly's heat shield along its trajectory is thoroughly studied. The decomposition of the solid as a function of temperature and the flow of pyrolysis gas through the material are added to evaluate their behavior along the trajectory. The results from the study show expected behavior, thereby determining the accuracy of the simulation. Based on the study, the next step is to run a multi-dimensional material response simulation which would include the tile scheme, as well as the gap-fillers.

5. Acknowledgement

Funding for this project is provided through NASA STRI Award 80NSSC21K1117 (E. Stern, Technical Monitor).

References

[1] Bowman, W. H. and Lawrence, R. M., "Ablative materials for high-temperature thermal protection of space vehicles," *Journal of Chemical Education*, Vol. 48, No. 10, October 1971, pp. 690–691.

[2] Sharp, J. R. and Page, A. T., "Ablation Modeling of ARES-I Upper Stage Thermal Protection System Using Thermal Desktop," *Thermal/Fluids Analaysis Workshop*, Cleveland, Ohio, September 2007.

[3] Brandis, A. M., Saunders, D. A., Allen, G., Stern, E. C., Wright, M. J., Mahzari, M., Johnston, C. O., Hill, J., Adams, D., and Lorenz, R., "Aerothermodynamics for Dragonfly's Titan Entry," Presentation ARC-E-DAA-TN57170, NASA, Boulder, Colorado, June 2018.

[4] Banerjee, A., Martin, A., and Poovathingal, S. J., "Estimating Effective Radiative Properties and In-Depth Radiative Heating of Porous Ablators," *AIAA SciTech Forum 2022*, AIAA Paper 2022-1640, San Diego, California, January 2022.

[5] Sirmalla, P. R., Chiodi, R., Panesi, M., and Bodony, D. J., "Fully Coupled Material Response Solver using Radiative Transfer for Thermal Protection Systems," *AIAA Aviation 2022 Forum*, AIAA Paper 2022-4005, Chicago, Illinois, June 2022.

[6] Weng, H. and Martin, A., "Multidimensional modeling of pyrolysis gas transport inside charring ablative materials," *Journal of Thermophysics and Heat Transfer*, Vol. 28, 10 2014, pp. 583–597.

[7] Weng, H., Ümran Düzel, Fu, R., and Martin, A., "Geometric effects on charring ablator: Modeling the full-scale stardust heat shield," *Journal of Spacecraft and Rockets*, Vol. 58, 2021, pp. 302–315.

[8] Zibitsker, A. L., McQuaid, J. A., Brehm, C., and Martin, A., "Development and Verification of a Mesh Deformation Scheme for a Three Dimensional Ablative Material Solver," *AIAA SciTech Forum*, AIAA Paper 2022-1285, Jan 2022.

[9] Cooper, J. M., Schroeder, O. M., Weng, H., and Martin, A., "Implementation and Verification of a Surface Recession Module in a Finite Volume Ablation Solver," *12th AIAA/ASME Joint Thermophysics and Heat Transfer Conference*, AIAA Paper 2018-3272, Atlanta, GA, June 2018.

[10] Davuluri, R. S. C., Fu, R., Tagavi, K. A., and Martin, A., "Fully coupled internal radiative heat transfer for the 3D material response of heat shield," *AIAA Aviation*, AIAA Paper 2021-3131, Virtual Event, Aug 2021.

[11] Davuluri, R. S. C., Rui Fu, K. A. T., and Martin, A., "Numerical investigation on the effect of spectral radiative heat transfer within an ablative material," *AIAA SciTech Forum*, AIAA Paper 2022-1283, San Diego, CA, Jan 2022.

[12] Martin, A. and Panesi, M., "Radiative transmission and absorption within the thermal protection system of an atmospheric entry spacecraft," *Journal of Spacecraft and Rockets*, Vol. 59, No. 10, 2022, pp. 348–352.

[13] Niemann, H. B., Atreya, S. K., Bauer, S. J., Carignan, G. R., Demick, J. E., Frost, R. L., Gautier, D., Haberman, J. A., Harpold, D. N., Hunten, D. M., Israel, G., Lunine, J. I., Kasprzak, W. T., Owen, T. C., Paulkovich, M., Raulin, F., Raaen, E., and Way, S. H., "The abundances of constituents of Titan's atmosphere from the GCMS instrument on the Huygens probe," *Nature*, Vol. 438, No. 7069, 2005, pp. 779–784.

[14] Lachaud, J., van Eekelen, T., Bianchi, D., and Martin, A., "TACOT v3.0," *Ablation Workshop: Code Comparison*, 4, 2014.